

New Methods for Image De-noising and Edge Enhancement in Cervical Smear Images Segmentation

¹Chuin-Mu Wang, ²Huang-Tsun Chen, ³Shys-Fan Yang-Mao, ^{4*}Yung-Kuan Chan
and ⁵Sheng-Fuu Lin

Abstract

The segmentation of cytoplasm and nucleus from a cervical cell image is one of important techniques for automatically detecting abnormal cervical cells. Noise on an image often makes segmentation inaccurate. This paper presents two new techniques, named trimming-mean filter and bi-grouping enhancer, to effectively eliminate noise and make the object boundaries more discernible. In this paper, the two proposed techniques are integrated with other techniques to create a nucleus and cytoplasm contour detector (NCCD detector) to automatically server the cytoplasm and nucleus from a cervical smear image. Compared to the gradient vector flow active contour model (GVF-ACM) and a texture-based segmentation method, the NCCD detector has a better performance in segmentation. Five commonly used performance criteria, including misclassification error (ME), edge mismatch (EM), region nonuniformity (RU), relative foreground area error (RFAE), and shape distortion penalty (SDP), will be taken to evaluate the segmentation techniques. The experimental results indicate that the NCCD detector is more effective in segmenting nucleus and cytoplasm from a cervical smear image.

Keywords: cervical smear screening, image segmentation, salt and pepper noise, Gaussian noise, active contour model

1. Introduction

The primary cause of mortality among women in Taiwan was cervical cancer before 1984. After the Taiwanese government encouraged women to undergo routine smear screening from 1996 to 2004, the death rate decreased to a fifth and is still decreasing [20]. Currently, smear screening is the most popular and efficient method to detect the abnormal cervical cells. The purpose of the screening is to diagnose pre-malignant cell changes before the cell progresses to a cancerous one.

*Corresponding Author: Yung-Kuan Chan
(E-mail: ykchan@nchu.edu.tw).

¹Department of Electronic Engineering, National Chin-Yi University of Technology, Taichung, Taiwan

²Department of Electrical and Control Engineering at National Chiao Tung University, Hsinchu, Taiwan

³Department of Computer Science, ⁴Department of Management Information Systems, and ⁵Department of Electrical Engineering, National Chung Hsin University, Taichung, Taiwan

Dysplasia cells have undergone precancerous changes, which generally have longer and darker nucleus and have a tendency to cling together in large clusters. It can be further divided into three stages — mild, moderate, and severe. Mild dysplasia cells are enlarged and have bright nuclei while the moderate dysplasia cells have larger and darker nuclei. The mild and moderate dysplasia cells may start to deteriorate and become severe dysplasia cells that have a large, dark, and often oddly shaped nucleus, dark cytoplasm, and is a relatively small cell [17]. Precancerous and cancerous cells are associated with a variety of morphologic and architectural alterations, including changes in cytoplasm and nucleus like brightness, roundness, size, elongation, perimeter, as well as the ratio of the cytoplasm area to the nucleus area. Figure 1 shows the examples of normal and abnormal squamous cells stained to enhance the image contrast.

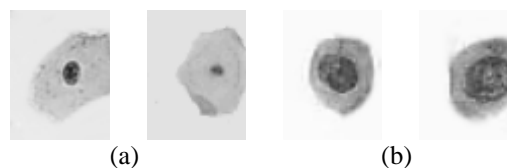


Figure 1: Squamous cells stained to enhance image contrast for (a) normal cells and (b) abnormal cells.

Currently, manual screening methods are costly and sometimes prone to human errors that often result in inaccurate diagnosis. Introduction of machine assisted screening techniques will bring significant benefits to the community, not only reducing financial costs but increasing screening accuracy. Efficient segmentation of cell nucleus and cytoplasm is crucial in designing an assisted screening system.

Wu et al. [25] introduced a parametric optimal segmentation approach which is suitable for the images of non-overlapped cells with smooth cell boundaries or contours. To conduct the segmentation of cell images, a priori knowledge of the nuclear characteristics is critical, which includes the shape, size of the cell, and its intensities relative to its background.

Mat-Isa et al., based on thresholding, [18] utilized the region growing algorithm as a feature extraction technique. This proposed algorithm is called seeded region growing features extraction (SRGFE), which is used to extract the size and grey level of certain region of interest on a digital image. In the SRGFE

algorithm, the user needs to determine the region of interest by clicking the mouse on any pixels in the region and to specify the threshold value, which makes the system impractical.

Walker [26] used a series of automated fast morphological transforms with octagonal structuring elements. Each gray-scale cell image is first globally thresholded, resulting in an incomplete segmentation of the nucleus in binary form. Cytoplasmic backgrounds are removed by performing a closing of the image using a structured element smaller than a minute nucleus, and nuclear inhomogeneity is corrected by an opening of a similar size. However, it is only suitable for local thresholding because it is not fully automated.

Many other cytoplasm and nucleus morphological segmentation methods have been proposed in the related literatures [1-5, 8, 10, 12-13, 16, 18, 25-26, 29]. However, most of their results are based on tedious hand-segmentation of images. Martin [17] and Norup [19] take the CHAMP Digital image software to segment and classify cervical smear images. Unfortunately, the CHAMP Digital image software cannot provide a satisfied segmentation performance, especially for abnormal cervical cells. The aim of this paper is to develop an image segmentation system to sever the cytoplasm and nucleus from a cervical smear image. This system is very helpful for—developing an automated cervical smear screening system without a priori knowledge of the image objects.

Generally, the accuracy of an object contour detector depends on the quality of the image. The heavily stained cervical smear may be masked by menstrual blood, vaginal discharge, air artifacts etc., obscure to the abnormal cervical cells. Sometimes, overexposure or underexposure under the microscope light may also blur the cervical smear images. This brings about difficulties for cytopathologists to extract important morphologies of cervical cells due to these problems.

The principal objective of image preprocessing techniques is to make an image more suitable than the original image for further processing. Noises on an image may obstruct object segmentation, but the denoising operation often introduces observable blurring effects. To resolve the problems mentioned above, in this paper, two new techniques — trim-meaning filter and bi-grouping enhancer — are presented to eliminate the noises on an image and to sharpen the object contours before extracting the objects. This paper also proposes a nucleus and cytoplasm contour detector (NCCD detector) to automatically segment the cytoplasm and nucleus from a cervical smear image for further analyses.

The NCCD detector takes the trimming-mean filter to dispose of the impulse and Gaussian noises in a cervical smear image I , while the bi-grouping enhancer is applied to sharpen the blur contours of the objects in I . Additionally, Sobel operator [11] is

adopted to compute the gradient map in I . An automatic thresholding method proposed by Otsu [21] is applied to find the gradient thresholds. A thinning algorithm [15] is used to trim off the false contour pixels. Finally, the darkest segmented object, regarded as the nucleus, in a cell is effectively separated from the cytoplasm. Besides cervical smear images, the trim-meaning filter and bi-grouping enhancer are also available in detecting object contours on other images.

2. NCCD Detector

Most image segmentation methods perform well when the image quality is good enough for our human vision to distinguish the contours of the objects. However, many cervical smear images are contaminated so that the contours between cytoplasm and nuclei of the cervical cells are often vague, especially for abnormal cells. This paper applies the trim-meaning filter and bi-grouping enhancer in pre-processing steps to eliminate the noises and to highlight the contours of the objects on an image. Based on both proposed techniques, this paper provides the NCCD detector. This section will introduce the NCCD detector in detail.

2.1 Image Denoising

The efficiency of object segmentation mainly depends on the quality of the processed image. It is well known that the generation of an accurate edge map becomes a critical issue when the images are corrupted by noises. Impulse (also known as salt & pepper) and Gaussian noises are frequently encountered during image acquisition. A Gaussian noise is the pixel with amplitude slightly different from that of its neighbors, while an impulse noise is the pixel with amplitude much larger or much smaller than those of its neighbors. This paper proposes a trimming-mean filter to remove the impulse noise and Gaussian noise which frequently occurred in the cervical smear images.

The trimming-mean filter works as follows. Let p_{ij} be the pixel located at position (i, j) in a cervical smear image I_o , and W_{ij} represent a window consisting of $m \times m$ pixels where p_{ij} is located at its center. We call W_{ij} is the corresponding window of p_{ij} . Assume that $C_{i,j} = \{c_1, c_2, \dots, c_{m^2}\}$ represents the colors of the pixels in W_{ij} , and the colors in $C_{i,j}$ are sorted in ascending order, $c_1 \leq c_2 \leq \dots \leq c_{m^2}$.

Since impulse noises are generally a few pixels with amplitudes much larger or smaller than those of their neighbors, the colors close to the lower and upper tails in $C_{i,j}$ may be the colors of impulse noises. Hence, the trimming-mean filter cuts off the lower and upper tails of $C_{i,j}$ for efficient removal of the impulse noise. In contrast, Gaussian noises are the

pixels with amplitudes only a little different from those of their neighbors. The trimming-mean filter eliminates Gaussian noise by replacing the color of p_{ij} with the average c' of the remaining pixel colors in C_{ij} . Both the impulse noise and Gaussian noise are expected to be eliminated effectively. Let α represent the percentage of pixels trimmed on the lower and upper tails of C_{ij} , and c' can be calculated from the following equation:

$$c' = \frac{1}{\alpha m^2} \sum \left\{ c_l \mid c_l \in C_k, l \in \left[I + \frac{(1-\alpha)m^2}{2}, \frac{(1+\alpha)m^2}{2} \right] \right\}$$

Figure 2 tells that the trimming-mean filter can significantly eliminate the impulsive and Gaussian noises, where α and m are set to be 0.5 and 5, respectively.

Several denoising techniques have been proposed, such as the average filter [14], the Gaussian filter [14] and type-B filter [23]. Figure 3 shows the images after eliminating the impulse noise and Gaussian noise using the previously mentioned filters. Figure 3(a) is a 64×64 synthetic image with the gray levels 125 and 175 in the central square and the surrounding areas, respectively. As shown in Figure 3(b), three percent of the impulse noises and Gaussian noises with parameter $\text{Sigma} = 4$ have been added to the image by using MATLAB image processing toolbox, **imnoise**. The PSNR between a noisy image and a denoised image is used to evaluate the efficacy of various denoising methods. As demonstrated in Figure 3, the trimming-mean filter can efficiently remove the impulse noise and Gaussian noise.

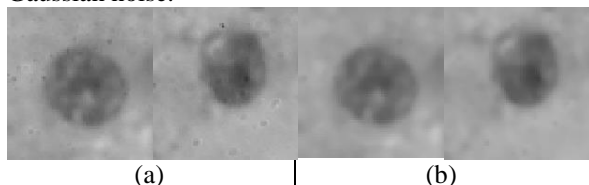


Figure 2: (a) The original cell images and (b) their corresponding images denoised by trimming-mean filter.

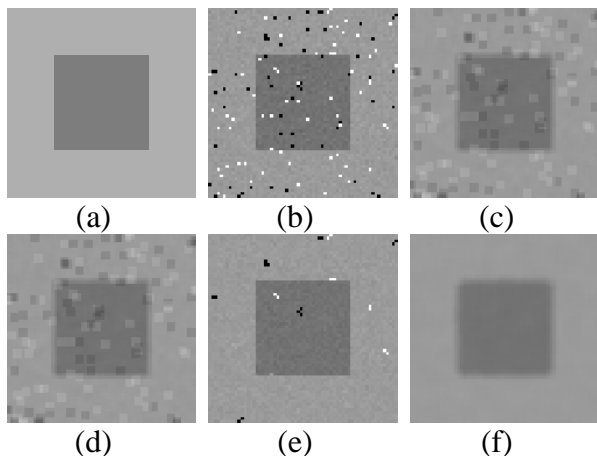


Figure 3: (a) The synthetic image and (b) its corresponding image corrupted by 3% impulse noises and Gaussian noises with the parameter $\text{Sigma} = 4$. The images after being processed by using (c) average filter, (d) Gaussian filter, (e) type-B filter, and (f) trimming-mean filter, respectively.

2.2 Edge Enhancement

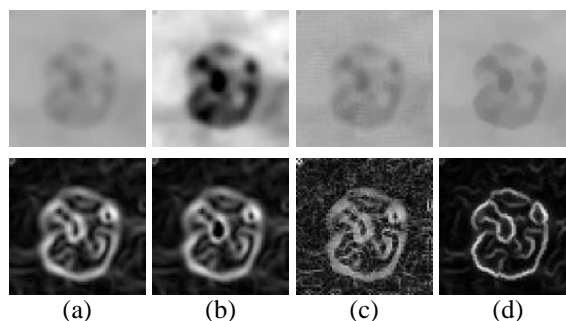


Figure 4: Cervical smear cell images (upper) and their corresponding gradient edge maps (lower). (a) The original images and the images after being processed by (b) AIO, (c) Type-A filter, and (d) bi-grouping enhancers

The term “edge” stands for a local luminance change, where the gradient of sufficient strength is considered important in a given task. Other contextual edge detection techniques based on edge suppression have been previously proposed. Russo [23] proposed a type-A filter to enhance the contours of objects by taking into account the differences between the pixel to be processed and its neighbors; small differences are considered as noises which should be reduced while large differences are treated as edges to be preserved. A two-step procedure is applied to each image channel to increase the effectiveness of smoothing action. Hence, type-A pixels are those corrupted by noises with amplitude similar to those of their neighbors.

Yin [28] also proposed an automatically adaptive window-level selection algorithm, namely adaptive image optimization (AIO), for improving the image quality. In this algorithm, the ROI is first extracted by using the variance change and the integral projection; second, the image statistics values, such as maximum, minimum, and average values, are obtained in the detected ROI; finally, the window and level are determined from the image statistics values, and a contrast transfer function is obtained using the cubic spline interpolation. Adopting AIO, the quality of the image is improved by increasing the maximum dynamic range adaptively.

Figure 4 shows the images processed by type-A filter and AIO algorithm, and their corresponding gradient images processed by Sobel gradient operator

[11]. The experiment results show that in both methods, suppression has no effect on nearby edges which have equally strong gradients. This paper therefore proposes bi-grouping enhancer to effectively isolate the object pixels from the background pixels.

In practice, there are many images with vague object boundaries, such as the images in Figures 4(a). Besides, denoising operations often introduce severe blurring effect. The purpose of the bi-grouping enhancer is to discriminate the object pixels from background pixels close to the contours of the objects.

After being processed by the trimming-mean filter, the original cervical smear image I_o becomes the image I_t . Similarly, let $p_{i,j}$ be the pixel located at the coordinates (i, j) in I_t , and $W_{i,j}$ be the corresponding window of $p_{i,j}$ where $p_{i,j}$ is the central pixel of $W_{i,j}$ consisting of $m \times m$ pixels. Assume that $C_{i,j} = \{c_1, c_2, \dots, c_{m^2}\}$ indicates the colors of the pixels in $W_{i,j}$ sorted in ascending order, $c_1 \leq c_2 \leq \dots \leq c_{m^2}$.

The bi-grouping enhancer defines the interval between $\frac{m^2-1}{2} \times \sum_{i=1}^{\frac{m^2-1}{2}} c_i$ and $c_{(m \times n + 1)/2-1}$ as well as the interval between $c_{(m \times n + 1)/2+1}$ and $\frac{m^2-1}{2} \times \sum_{i=\frac{m^2+3}{2}}^{m^2} c_i$ as indefinite intervals. It is difficult to recognize whether $p_{i,j}$ is in an object or in background while the color c of $p_{i,j}$ lies in both intervals.

Set $index = \left\lfloor \frac{m^2}{2} \right\rfloor$ and m to odd numbers. Hence, the bi-grouping enhancer replaces the grey level c of $p_{i,j}$ with c' , where c' is defined as:

$$c' = \begin{cases} \frac{1}{index} \sum_{i=1}^{index} c_i, & \text{if } \frac{1}{index} \sum_{i=1}^{index} c_i \leq c \leq \frac{1}{m^2} \sum_{i=1}^{m^2} c_i, \\ \frac{1}{index} \sum_{i=index}^{m^2} c_i, & \text{if } \frac{1}{m^2} \sum_{i=1}^{m^2} c_i \leq c \leq \frac{1}{index} \sum_{i=index}^{m^2} c_i, \\ c, & \text{otherwise} \end{cases}$$

If c is in the indefinite intervals, the bi-grouping enhancer changes c into the average c_a of the first half of $C_{i,j}$ when c is closer to c_a , or c is supplanted by the average of the latter half of $C_{i,j}$. Figures 5 illustrates that the bi-grouping enhancer can more efficiently separate the object pixels from the background pixels effectively.

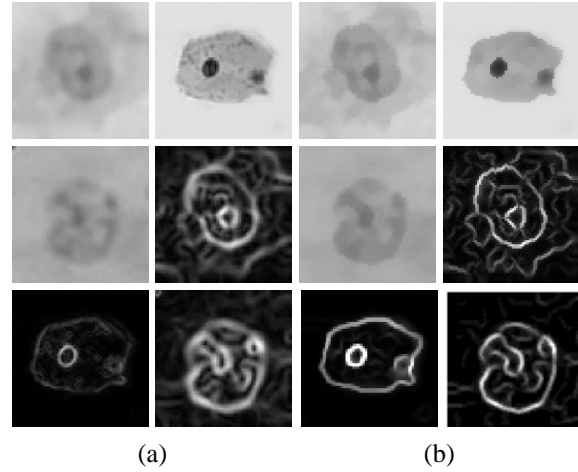


Figure 5: (a) Three original images and their gradients; (b) The images after being processed by the trimming-mean filter and their gradients after further being processed by the bi-grouping enhancer

2.3 Gradient Calculation

Since an edge corresponds to a set of strong illumination gradients, the edge can be displayed in colors by calculating the derivatives of the image. The position of the edge can be estimated with the maximum of the first derivative or with the zero-crossing of the second derivative. Many gradient computation methods have been proposed, such as the Matlab gradient function, Roberts cross, and the Sobel operator [11]. The Sobel operator is widely used and has proved to be efficient for the gradient edge detector. Thus, this paper takes the Sobel operator to compute the gradients of all the pixels in the image obtained by the bi-grouping enhancer. The Sobel operator performs a 2-D spatial gradient measurement on an image and emphasizes the regions of high spatial gradient corresponding to edges. Two 3×3 convolution masks shown in Figure 6 are employed in the Sobel operator.

Let $p_{i,j}$ be a pixel located at the coordinates (i, j) in the image, and $W_{i,j}$ be the corresponding window of $p_{i,j}$ with 3×3 pixels. The gradient $g_{i,j}$ of $p_{i,j}$ is defined as

$$g_{i,j} = ((G_x \oplus W_{i,j})^2 + (G_y \oplus W_{i,j})^2)^{1/2},$$

where \oplus is the operator of convolution. Assume that g_M is the maximal gradient of all the pixels in the image. To generate an image f_g describing the gradients of the pixels in the image, this approach assigns the value $\frac{g_{i,j}}{g_M} \times 255$ to the color intensity of the pixel located at the coordinates (i, j) in image f_g .

-1	0	+1
-2	0	+2
-1	0	+1

G_x

+1	+2	+1
0	0	0
-1	-2	-1

G_y

Figure 6: Sobel convolution masks G_x and G_y in the x- and y-directions

2.4 Threshold Finding

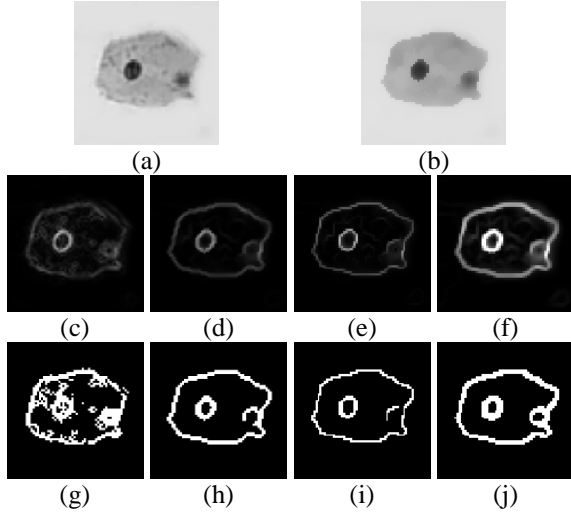


Figure 7: (a) A cervical image; (b) the image of (a) after being processed by the trimming-mean filter and the bi-grouping enhancer; (c) the gradient of (a) obtained by Matlab gradient function; (d) the gradient of (b) obtained by the Matlab gradient function; (e) the gradient of (b) obtained by Roberts cross; (f) the gradient of (b) obtained by the Sobel operator; (g), (h), (i), and (j) are respectively the f_b of (c), (d), (e), and (f)

The color intensity of a pixel p_{ij} in f_g represents the possibility of the pixel located at the coordinates (i, j) in f_0 to be an edge pixel. To successfully cut off the cytoplasm and nucleus from f_0 , given an adaptive threshold to isolate the possible edge pixels is the pre-requisite. When given a bigger threshold, higher contrast edges may be obtained but some desired low contrast edges may be missed. On the contrary, lower contrast edges may be earned for given a smaller threshold but more noise edges may probably be obtained at the same time. Otsu's method [21] is one of the often used threshold decision methods. The NCCD detector hence utilizes it to specify the threshold Th .

Assume that f_g contains n pixels with gray levels from 1 to l . Let n_i be the number of pixels at level i ; hence, $n=n_1+n_2+\dots+n_l$. Suppose that the pixels are dichotomized into two classes C_0 and C_1 , so that the gray levels of the pixels in C_0 and C_1 are respectively in the interval $[1, 2, \dots, l_0]$ and in the interval $[l_0+1, l_0+2, \dots, l]$. Otsu's method maximizes the posteriori

between-class variance $\sigma_B^2(t)$ by given the following equation:

$$\sigma_B^2(t) = \omega_0(t)\omega_1(t)[\mu_1(t) - \mu_0(t)]^2 = \omega_0(t)[1 - \omega_0(t)] \left(\frac{\mu_T - \mu_1(t)}{1 - \omega_0(t)} - \frac{\mu_1(t)}{\omega_0(t)} \right)^2,$$

where

$$\omega_0(t) = \sum_{i=1}^{l_0} \frac{n_i}{n},$$

$$\omega_1(t) = 1 - \omega_0(t),$$

$$\mu_0(t) = \sum_{i=1}^{l_0} \left(i \times \frac{n_i}{n} \right),$$

$$\mu_1(t) = \sum_{i=l_0+1}^l \left(i \times \frac{n_i}{n} \right), \text{ and}$$

$$\mu_T = \sum_{i=1}^l \left(i \times \frac{n_i}{n} \right).$$

The optimal threshold Th is found through a sequence of searches:

$$Th = \arg \left(\max_{t=2}^{l-1} (\sigma_B^2(t)) \right).$$

After that, the NCCD detector sweeps each pixel p_{ij} in f_g to generate a binary image f_b . If the color intensity of p_{ij} is greater than or equal to Th , the NCCD detector assigns 1 to be the color of the pixel located at the coordinates (i, j) on f_b ; otherwise it is given to be 0 . The pixels in f_g corresponding to the pixels colored by 1 in f_b are called candidate edge pixels. Figure 7 shows the gradients obtained by Matlab gradient function, Roberts cross, and the Sobel operator, and their f_b .

2.5 Nucleus and Cytoplasm Segmentation

The expected edge should be one-pixel thick. The NCCD detector hence adopts a hit-and-miss transform based skeletonization (HMTS) algorithm [15] to build the edges of thickness of one pixel. We name the eliminated candidate edge pixels redundant-edge pixels and the remaining candidate edge pixels true-edge pixels.

0	0	0	0	0	0	1	0	1	1
1	1	1	1	1	0	1	1	0	0
1	1	1	1	1	1	1	0	0	0
1	1	1	1	1	1	0	1	0	0
1	1	1	1	0	1	1	1	0	1
0	0	0	0	0	0	0	1	1	1

Figure 8: The eight structuring elements for thinning

In this paper, the HMTS algorithm is used to remove the redundant-edge pixels so that each edge's thickness is one pixel. Let each pixel p_{ij} in f_b correspond to a window W_{ij} , where W_{ij} consists of 3×3 pixels and p_{ij} be the central pixel of W_{ij} . This algorithm compares W_{ij} with each of the eight structuring elements shown in Figure 8 where the gray areas stand for don't-care pixels. A don't-care pixel may be a 1-bit pixel or a 0-bit pixel. We say W_{ij} is matched if the positions and values of the 1-bits and 0-bits on one structuring element are completely the same as those of W_{ij} regardless of don't-care pixels. When W_{ij} is matched, the color of p_{ij} is changed into 0.

The HMTS algorithm is performed to trim away the redundant-edge pixels, so that the edges are the thickness of only one pixel. It scans each pixel p_{ij} in f_b . If W_{ij} is match, p_{ij} is given to be 0-bit. The algorithm repeats this procedure until no more thinning has to be performed. The HMTS algorithm guarantees that connectivity is preserved so that the overall geometric structure of the object in the image is preserved.

However, uneven edges of objects tend to cause small spurs on the skeleton, which are not the required edges in this paper. Therefore, a pruning algorithm is required to remove them. The procedure of the pruning algorithm is entirely the same as those of the HMTS algorithm except for the eight structuring elements in Figure 8 are replaced by the eight structuring elements in Figure 9.

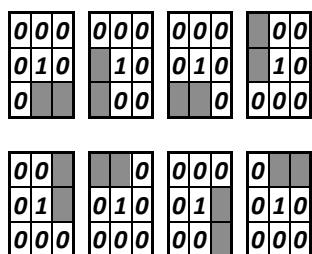


Figure 9: The eight structuring elements for trimming spurs

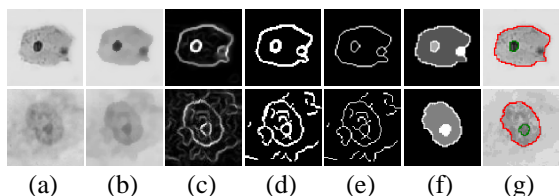


Figure 10: (a) Two cell images; the image obtained orderly by (b) trimming-mean filter and bi-grouping enhancer, (c) Sobel operator, (d) Otsu's thresholding, (e) thinning, (f) spur trimming, and (g) nucleus-cytoplasm segmentation

Finally, the biggest closed loop L_c on f_b describes the contour of the cytoplasm, and the darkest region on f_0 surrounded by a loop which corresponds to a closed loop L_n on f_b within L_c is the nucleus. It means that L_c and L_n are the cytoplasm and nucleus contours of the cervical cell on f_0 . Figure 11 shows the results obtained in each approach of the NCCD detector.

3. Experimental Results

The purpose of this section is to investigate the performance of the NCCD detector by experiments compared to the performances of the GVF-ACM method [27] and the CHAMP software [17, 19]. These experiments use of 25 gray-level cervical smear images as the test images, each with 64×64 pixels, where 12 were provided by Dr. Huang of the Taichung Hospital in Taiwan, R.O.C. and the remnants were downloaded from the cell image database from the Technical University of Denmark, DTU [17]. Figure 16 displays these test images and their target cytoplasm and nucleus contours, manually drawn by an experienced doctor.

In these experiments, the NCCD detector was employed to extract the cytoplasm and nucleus contours of the test images. It takes $m=5$ and $\alpha=0.5$ in trim-meaning approach, and $m=5$ in bi-grouping approach. The GVF-ACM method is adopted to sever the cytoplasts and nucleuses from the test images where all the parameters α, β, κ are given to be 1. The CHAMP software is also used to separate the cytoplasts and nucleuses from the test images. Figure 11 gives the cytoplasm and nucleus contours of the 25 test images cut by the NCCD detector, GVF-ACM method, and CHAMP software.

No.	Original Image	Target Contour	CHAMP	ACM-GV F	NCCD
1					
2					
3					
4					
5					

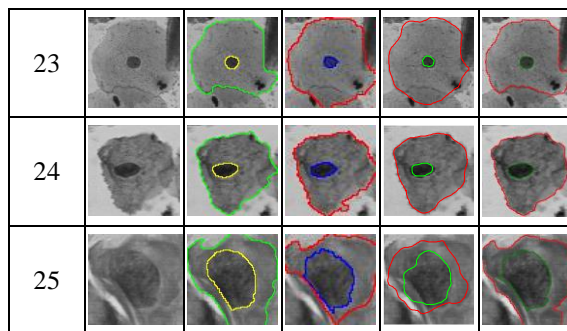
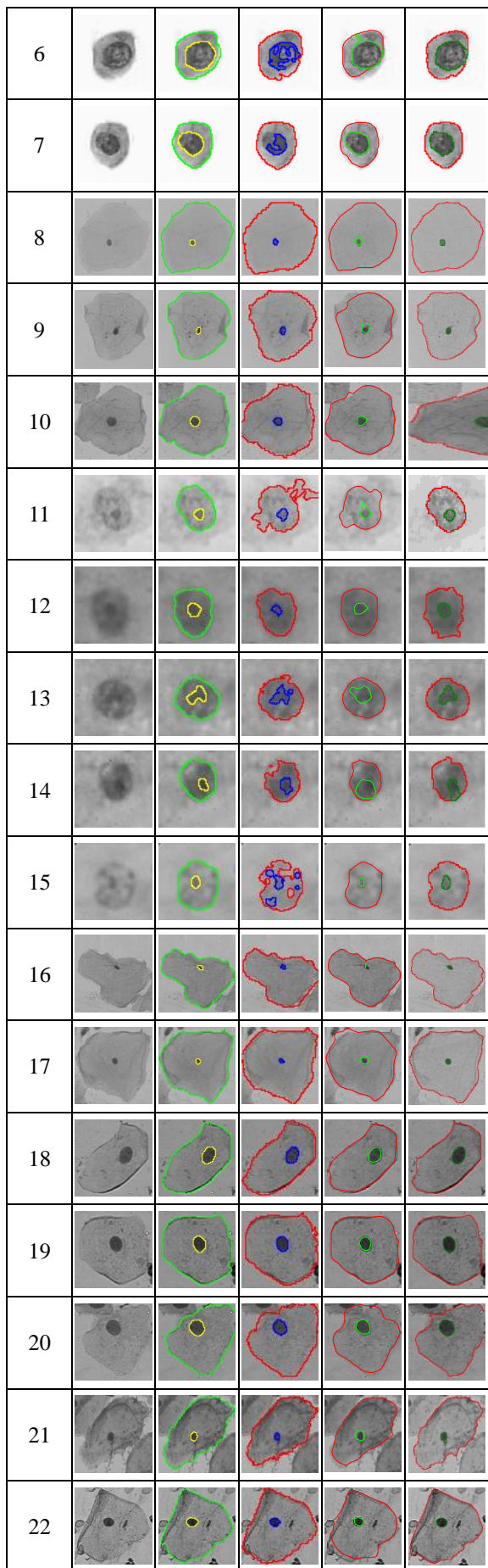


Figure 11: The original images, the target cytoplasm and nucleus contours of the test image, and the cytoplasm and nucleus contours cut by the CHAMP software, GVF-ACM method, and NCCD detector

Mehmet Sezgin and Bulent Sankur [24] survey five frequently used error measures of segmentation: misclassification error (ME), edge mismatch (EM), region nonuniformity (RU), relative foreground area error (RFAE), and shape distortion penalty (SDP). This paper also evaluates the performances of the CHAMP software, GVF-ACM method, and NCCD detector via ME, EM, RU, RFAE, and SDP. Table 1 respectively lists the averages (Ave) and standard deviations (Std) of the error measures for the extracted cytoplasm and nucleus contours of the 25 testing images cut by the CHAMP software, GVF-ACM method, and NCCD detector.

Table 1. The averages and standard deviations (Ave/Std) of the error measures for the extracted cytoplasm and nucleus contours obtained by the CHAMP software, GVF-ACM method, and NCCD detector

Method	Object	ME	EM	NU	RFAE	MHD
GVF-ACM	Nucleus	0.015/0.016	0.681/0.130	0.015/0.034	0.355/0.199	1.260/0.456
	Cytoplasm	0.079/0.064	0.554/0.221	0.100/0.112	0.124/0.124	1.436/0.978
CHAMP	Nucleus	0.011/0.014	0.399/0.174	0.011/0.036	0.249/0.170	0.512/0.357
	Cytoplasm	0.058/0.034	0.416/0.117	0.143/0.124	0.106/0.076	0.757/0.427
NCCD	Nucleus	0.002/0.004	0.0720/0.120	0.016/0.033	0.047/0.093	0.125/0.224
	Cytoplasm	0.008/0.010	0.048/0.067	0.109/0.106	0.020/0.032	0.143/0.215

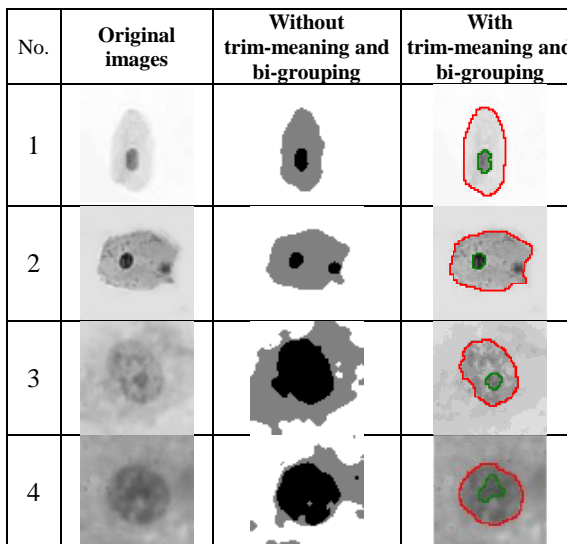




Figure 12: (a) The original images and their corresponding segmented images obtained by the methods (b) without the trim-meaning filter and bi-grouping enhancer, and (c) with the trim-meaning filter and bi-grouping enhancer

The GVF-ACM method is very sensitive to the curves of objects and noises. Hence, the GVF-ACM method cannot provide a satisfactory performance for segmenting the nucleuses and cytoplasts of most images in Figure 11. Although different results could be obtained by changing the values of its parameters, the optimal parameters are image-dependent. It is very difficult to specify a set of parameters which can be applied to all of the images. The CHAMP software works very well, such as, the images 2, 3, 5, 8, 17, 21 in Figure 11, when the texture of an object is uniformed. Otherwise, it gives unsatisfactory results, for example, the images 6, 7, 11-15 in Figure 11. Table 1 and Figure 11 demonstrate that normally the NCCD detector can provide a much better performance in segmenting cytoplasm and nucleus.

The next experiment is to scrutinize the performance of the trim-meaning filter and bi-grouping enhancer. In this experiment, Otsu's method is used to find the adaptive threshold for isolating the possible edge pixels on the original images in Figure 12 without the pre-processed by the trim-meaning filter and bi-grouping enhancer. The images in column "Without trim-meaning and bi-grouping" of Figure 12 are the experimental results. Additionally, the images in column "With trim-meaning and bi-grouping" of Figure 12 are the results obtained by the NCCD detector.

4. Conclusions

This paper presents a NCCD detector to automatically extract the cytoplasm and nucleus of a cervical smear image. Noises on an image often make segmentation inaccurate. This paper provides the trimming-mean filter to eliminate the noises on an image, and the bi-grouping enhancer to suppress the noises and brighten the object contours. These two proposed techniques are then integrated with the Sobel operator, Otsu's method, HMTS algorithm, and pruning algorithm, to create the NCCD detector automatically detecting the cytoplasm and nucleus contours of a cervical smear image.

This paper also takes five frequently used error measures of segmentation to evaluate the efficiency of segmentation obtained by the CHAMP software, GVF-ACM method, and NCCD detector. The

experimental results show that the NCCD detector can give much better segmentation effectiveness than the CHAMP software and GVF-ACM method. The experimental results also show that the trimming-mean filter and the bi-grouping enhancer are much helpful to eliminate noises and intensify the contour of an object. Besides the cervical smear image, the trimming-mean filter and the bi-grouping enhancer can be also valuable for detecting the object contours on other images.

References

- [1] P. Bamford, and B. Lovell, "A Water Immersion Algorithm for Cytological Image Segmentation," In APRS Image Segmentation Workshop, Sydney, Australia, December 13, 1996, pp. 75-79.
- [2] P. Bamford, and B. Lovell, "Unsupervised Cell Nucleus Segmentation with Active Contours," Signal Processing - Special issue on Deformable Models and Techniques for Image and Signal Processing, 1998, pp. 203 – 213.
- [3] P. Bamford, and B. Lovell, "Improving the Robustness of Cell Nucleus Segmentation," Proceedings of British Machine Vision Conference, Vol. 2, Southampton, UK, September 14-17, 1998, pp 518-524.
- [4] P. Bamford, and B. Lovell, "A Methodology for Quality Control in Cell Nucleus Segmentation," In Digital Image Computing: Techniques and Applications, Perth, Australia, December 7-8, 1999, pp. 21-25.
- [5] P. Bamford, and B. Lovell, "Method for Accurate Unsupervised Cell Nucleus Segmentation," In IEEE Engineering in Medicine and Biology, Istanbul, Turkey, October 25-28, 2001, pp. 2704-2708.
- [6] J. Canny, "A Computational Approach to Edge Detection," IEEE Transactions on Pattern Analysis and Machine Intelligence, Vol. 8, No. 6, November, 1986, pp. 679-698.
- [7] D. Comaniciu, and P. Meer, "Mean Shift Analysis and Applications," IEEE International Conference on Computer Vision, Kerkyra, Greece, 1999, pp. 1197-1203.
- [8] D. Comaniciu, and P. Meer, "Cell Image Segmentation for Diagnostic Pathology," in Advanced Algorithmic Approaches to Medical Image Segmentation: State-of-The-art Applications in Cardiology, Neurology, Mammography and Pathology, Springer, New York, NY, USA, 2001, pp. 541-558.
- [9] D. A. Clausi, and B. Yue, "Comparing Cooccurrence Probabilities and Markov Random Fields for Texture Analysis of SAR Sea Ice Imagery," IEEE Transactions on Geoscience and Remote Sensing, Vol. 42, No. 1, January 2004, pp. 215-228.

- [10] Y. F. Chen, J. R. Liao, and S. J. Chen, "The Application of Gradient Vector Flow Active Contour Model in the Detection of Cervical Cells Obtained from Pap Smears," Proceedings of the International Conference on Mathematics and Engineering Techniques in Medicine and Biological Sciences, Las Vegas, 2004, pp.58-63.
- [11] E. Davies, "Machine Vision: Theory, Algorithms and Practicalities, Second Edition, San Diego, Academic Press, 1996.
- [12] V. Dadeshidze, L. Olsson, and R. A. Domanik, "Segmentation of Nuclear Images in Automated Cervical Cancer Screening," Proceedings of SPIE for Optical Engineering, Vol.2622, 1995, pp.723-727.
- [13] G. Fernandez, M. Kunt, and J. P. Zryd, "A New Plant Cell Image Segmentation Algorithm," Proceedings of the 8th International Conference on Image Analysis and Processing, San Remo, Italy, 1995, pp. 229-234.
- [14] R. Gonzalez, and R. Woods, "Digital Image Processing", 2nd Edition by Gonzalez and Woods, Prentice-Hall, 2002.
- [15] L. Lam, S. W. Lee, and C. Y. Suen, "Thinning Methodologies-A Comprehensive Survey," IEEE Transactions on Pattern Analysis and Machine Intelligence, Vol. 14, No. 9, September 1992, pp. 869 – 885.
- [16] Y. Liu, T. Zhao, and J. Zhang, "Learning Multispectral Texture Features for Cervical Cancer Detection," Proceedings of IEEE International Symposium on Biomedical Imaging: Macro to Nano, Washington D.C., July 2002, pp. 169–72.
- [17] E. Martin, "Cervical smear Classification," Master's Thesis, Technical University of Denmark: Oersted-DTU, Automation, 2003.
- [18] N. A. Mat-Isa, M. Y. Mashor, and N. H. Othman, "Seeded Region Growing Features Extraction Algorithm; Its Potential Use in Improving Screening for Cervical Cancer," International Journal of The Computer, the Internet and Management, Vol. 13, No. 1, January-April 2005, pp 61 -70.
- [19] J. Norup, "Classification of Cervical Smear Data by Transductive Neuro-Fuzzy Methods," Master's Thesis, Technical University of Denmark: Oersted-DTU, Automation, 2005.
- [20] National Health Insurance, Cause of Mortality Report, Health and National Health Insurance statistics information, <http://www.doh.gov.tw/statistic/>, 2004.
- [21] N. Otsu, "A Threshold Selection Method from Gray-Level Histograms," IEEE Transactions on Systems, Man, and Cybernetics, Vol. 9, No. 1, 1979, pp. 62-66.
- [22] R. S. Poulsen, and I. Pedron, "Region of Interest Finding in Reduced Resolution Colour Imagery - Application to Cancer Cell Detection," Pattern Recognition, Vol. 28, No. 11, 1995, pp. 1645-1655.
- [23] F. Russo, and A. Lazzari, "Color Edge Detection in Presence of Gaussian Noise Using Nonlinear Prefiltering," IEEE Transactions on Instrumentation and Measurement, Vol. 54, No. 1, February 2005, pp. 352-8.
- [24] M. Sezgin, and B. Sankur, "Survey Over Image Thresholding Techniques and Quantitative Performance Evaluation," Journal of Electronic Imaging, Vol. 13, No. 1, January 2004, pp. 146–165.
- [25] H. S. Wu, J. Gil, and J. Barba, "Optimal Segmentation of Cell Images," IEE Proceedings - Vision, Image, and Signal Processing, Vol. 145, No 1, February 1998, pp. 50-56.
- [26] R. F. Walker, "Adaptive Multi-Scale Texture Analysis with Application to Automated Cytology," PhD. Dissertation, Department of Electrical and Computer Engineering, University of Queensland, Australia, 1997.
- [27] C. Xu, and J. L. Prince, "Snakes, Shapes, and Gradient Vector Flow," IEEE Transactions on Image Processing, Vol. 7, No. 3, March 1998, pp. 359-369.
- [28] L. Yina, A. Basub, and J. K. Changc, "Scalable Edge Enhancement with Automatic Optimization for Digital Radiographic Images," Pattern Recognition, Vol. 37, No. 7, July 2004, pp. 1407–1422.
- [29] Y. J. Zhang, "A Survey on Evaluation Methods for Image Segmentation," Pattern Recognition, Vol. 29, No. 8, August 1996, pp. 1335–1346.